Pergamon

Tetrahedron 58 (2002) 3911–3922

TETRAHEDRON

Fluorous derivatives of [Rh(COD)(dppe)]BX_4 (X=F, Ph): synthesis, physical studies and application in catalytic hydrogenation of 1-alkenes and 4-alkynes

Elwin de Wolf,[a] Anthony L. Spek,[b] Bonny W. M. Kuipers,[c] Albert P. Philipse,[c] Johannes D. Meeldijk,[d] Paul H. H. Bomans,[e] Peter M. Frederik,[e] Berth-Jan Deelman[f,*] and Gerard van Koten[a]

[a]*Department of Metal-Mediated Synthesis, Debye Institute, Utrecht University, Padualaan 8, CH-3584 Utrecht, The Netherlands*
[b]*Department of Crystal- and Structural Chemistry, Bijvoet Centre for Biomolecular Research, Utrecht University, Padualaan 8, CH-3584 Utrecht, The Netherlands*
[c]*Van't Hoff Laboratory for of Physical and Colloid Chemistry, Debye Institute, Utrecht University, Padualaan 8, CH-3584 Utrecht, The Netherlands*
[d]*Debye Institute, Utrecht University, Padualaan 8, CH-3584 Utrecht, The Netherlands*
[e]*EM-unit, Universiteit Maastricht, P.O. Box 616, MD-6200 Maastricht, The Netherlands*
[f]*ATOFINA Vlissingen B.V., P.O. Box 70, AB-4380 Vlissingen, The Netherlands*

Received 31 October 2001; revised 21 February 2002; accepted 22 February 2002

Abstract—Fluorous derivatives of 1,2-bis(diphenylphosphino)ethane (dppe) (**1**), containing a *para*-(1*H*,1*H*,2*H*,2*H*-perfluoroalkyl)silyl function, were used in the synthesis of fluorous derivatives of [Rh(COD)(dppe)]BF_4. The single crystal X-ray crystallographic structure of [Rh(COD)(**1a**)]BPh_4 (**7**) was determined (**1a**=[$CH_2P(C_6H_4$–$SiMe_2CH_2CH_2C_6F_{13}$-*p*)$_2$]$_2$). Large differences in catalytic activity and selectivity (higher hydrogenation activity and lower isomerization activity) relative to [Rh(COD)(dppe)]BF_4 were observed in the hydrogenation of 1-octene using non-fluorous, silyl-substituted [Rh(COD)(**2**)]BF_4 (**5**; **2**=[$CH_2P(C_6H_4$–$SiMe_3$-*p*)$_2$]$_2$ or [Rh(COD)(**3**)]BF_4 (**6**; **3**=[$CH_2P(C_6H_4$–$SiMe_2C_8H_{17}$-*p*)$_2$]$_2$) and even more so with fluorous [Rh(COD)(**1a**)]BF_4 (**4a**). For **4a** and **6**, the presence of aggregates was demonstrated by dynamic light scattering (DLS) and cryogenic transmission electron microscopy (cryoTEM), which is most probably responsible for these differences. Similar differences between (fluorous) silylated catalysts and non-substituted [Rh(COD)(dppe)]BF_4 were observed in the semi-hydrogenation of 4-octyne. Recycling of highly fluorous catalyst [Rh(COD)(**1c**)]BF_4 (**4c**; **1c**=[$CH_2P(C_6H_4$-$Si(CH_2CH_2C_6F_{13})_3$-*p*)$_2$]$_2$) was investigated in two different fluorous biphasic solvent systems. The catalyst could be recycled with 97.5% (for PFMCH/acetone, 1:1 v/v) and >99.92% (for FC-75/hexanes, 1:3 v/v) retention of rhodium, respectively. The leaching of phosphorus was comparable to the leaching of rhodium (in PFMCH/acetone), showing that dissociation and leaching of free ligand does not take place for these rhodium diphosphine catalysts.

1. Introduction

Diphosphine transition metal complexes are widely used as catalyst in several types of homogeneous catalysis.[1] Since these complexes often contain expensive metals and (chiral) ligands, recycling of these complexes by fluorous phase separation techniques is of major interest.[2] Only a few transition metal complexes containing fluorous bidentate phosphine ligands are known in the literature,[3] all of which display suboptimal catalytic activity.[4] Also, to the best of our knowledge, only two fluorous phase-soluble ionic complexes have been reported. These employ fluorous derivatives of the 2,4-pentanedionate anion or $(MeO)_2PCH_2CH_2P(OMe)_2$ as ligand, i.e. K[Ru{$(F_{15}C_7)$-C(O)CHC(O)(C_7F_{15})}$_3$] and in situ generated [Rh(COD){$CH_2P(OCH_2CH_2C_6F_{13})_2$}$_2$]OTf, respectively.[5] Possibly, even higher fluorous character is necessary to dissolve these ionic complexes in fluorous solvents, since in fluorous solvents with low dielectric constant, strong solvent–solute interactions needed to separate ion pairs are lacking. For neutral fluorous bidentate phosphine complexes it was previously noted that at least eight perfluoroalkyl tails are necessary to achieve good solubility in fluorous solvents.[3]

The use of the $-SiMe_{3-b}(CH_2CH_2-)_b$ spacer (b=1–3)[6] enabled us to synthesize fluorous derivatives of 1,2-bis-(diphenylphosphino)ethane (**1a–c**) containing up to 12 tails per molecule.[7] Here, we report the use of diphosphines **1–3** in the synthesis of rhodium complexes, along with a

Keywords: fluorous biphasic catalysis; catalyst recycling; phosphine; hydrogenation; rhodium.
* Corresponding author; e-mail: b.j.deelman@chem.uu.nl

0040–4020/02/$ - see front matter
PII: S0040-4020(02)00217-X

Table 1. NMR data of $[Rh(COD)(dppe)]BF_4$ and its silyl-substituted (non)fluorous derivatives

Compound	^{31}P NMR δ (ppm)[a]	$^{1}J_{RhP}$ (Hz)	^{103}Rh NMR δ (ppm)[a]
$[Rh(COD)(dppe)]BF_4$	56.5	148.4	−513
5	56.4	148.4	−512
6	56.4	148.3	–
4a	56.5	148.3	−509
4b[b]	56.8	149.3	–
4c[c]	57.5	148.3	–
7	56.1	148.4	–

[a] In $CDCl_3$, unless noted otherwise.
[b] In $C_6D_6/CF_3C_6H_5$, 1:1 (v/v).
[c] In C_6D_6/FC-72, 1:1 (v/v).

single crystal X-ray crystallographic study of [Rh(COD)-(**1a**)]BPh_4. These novel complexes were applied as catalyst precursors in the hydrogenation of 1-alkenes and alkynes. Moreover, their recycling using fluorous biphasic separation was investigated. The large differences in catalytic performance observed between the fluorous complexes and their non-fluorous counterparts stimulated us to study the steric and electronic effects imposed by the perfluoroalkyl substitution as well as the aggregation behavior of these complexes in polar solvents. To investigate the shape and size of any aggregates, both dynamic light scattering (DLS) and cryogenic transmission electronmicroscopy (cryoTEM) were employed.

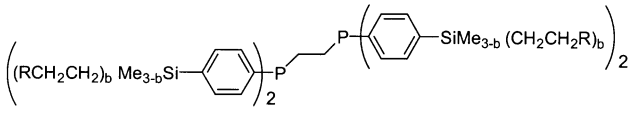

1 - 3

1a: R = C_6F_{13}, *b* = 1
1b: R = C_6F_{13}, *b* = 2
1c: R = C_6F_{13}, *b* = 3
2: *b* = 0
3: R = C_6H_{13}, *b* = 1

2. Results and discussion

The fluorous complexes [Rh(COD)(**1a**–**c**)]BF_4 (**4a**–**c**), trimethylsilyl-substituted [Rh(COD)(**2**)]BF_4 (**5**), dimethyl-(octylsilyl) substituted [Rh(COD)(**3**)]BF_4 (**6**) and [Rh(COD)(**1a**)]BPh_4 (**7**) were synthesized from $[Rh(COD)_2]BF_4$ or [Rh(acac)(COD)], respectively, following slightly modified literature procedures.[8] All compounds were identified by both ^1H and ^{31}P NMR spectroscopy and elemental analyses and in some cases also by ^{19}F NMR spectroscopy (**4a**,**b**, **5**). ^1H NMR spectra of **4b** and **c** at room temperature in C_6D_6/FC-72 (1:1 v/v) (FC-72 is mixture of perfluorohexanes) as solvent system displayed broad peaks with unresolved multiplicities.[9]

The ^{31}P NMR chemical shifts and the $^1J_{RhP}$ coupling constants of **4**, **5**, **6** and **7** were found to be in close agreement with data found for non-substituted [Rh(COD)-(dppe)]BF_4 (Table 1). Also, the ^{103}Rh NMR chemical shifts of [Rh(COD)(dppe)]BF_4, **4a** and **5** were found to be very similar. It is known that the ^{103}Rh NMR chemical shift is a very sensitive probe for both electronic and steric influences_.[10] For example, shifts of 20–100 ppm are observed upon small geometrical variations (P–Rh–P bite angle, Rh–P distance etc.). Therefore, the similarity of the ^{103}Rh NMR chemical shifts of [Rh(COD)(dppe)]BF_4, **4a** and **5** indicates that both the *para*-trimethylsilyl and a *para*-(1*H*,1*H*,2*H*,2*H*-perfluoroalkyl)dimethylsilyl substituents have no significant consequences for the electronic environment and/or coordination geometry of the respective rhodium centers.

Interestingly, single crystals of [Rh(COD)(**1a**)]BPh_4 (**7**) suitable for X-ray structural analysis were obtained. Complex **7** is, to the best of our knowledge, the first fluorous diphosphine–metal complex of which the molecular structure has been studied by single crystal X-ray crystallography and is one of the few crystal structures of perfluoroalkylated phosphine complexes that have been reported.[11] An ORTEP representation showing the molecular geometry of **7** in the solid state is presented in Fig. 1. Selected bond lengths and angles as well as torsion angles are given in Table 2. Unfortunately, this structure cannot be directly compared with its non-fluorous analogue [Rh(COD)(dppe)]X (X=a weakly coordinating anion), since no examples of these compounds have been studied crystallographically. Therefore, comparison is made with rhodium–COD complexes containing other ethanediyl bridged diphosphine ligands.

Rh–P bond lengths (2.273(9) and 2.272(8) Å) are similar to reported values for $[Rh(COD)(L_2)]^+$ (average Rh–P distance=2.27 Å for L_2=CHIRAPHOS, DiPAMP or DuPHOS).[12] The P–Rh–P bite angle (82.4(3)°) of **7** is at the low end of the range observed for the above mentioned

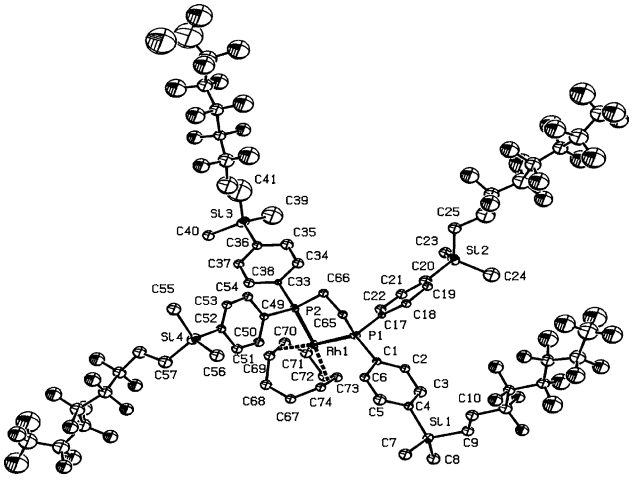

Figure 1. ORTEP drawing of **7** at 30% probability level. Hydrogen atoms and the BPh_4^- residue are omitted for clarity.

Table 2. Selected bond lengths (Å), angles (°) and torsion angles (°) with estimated standard uncertainties in parentheses for [Rh(COD)(**1a**)]BPh_4 (**7**)

Rh(1)–P(1)	2.273(9)	C(69)–C(70)	1.35(4)
Rh(1)–P(2)	2.272(8)	C(73)–C(74)	1.41(4)
Rh(1)–C(69)	2.22(3)	C(59)–C(60)	1.47(3)
Rh(1)–C(70)	2.26(3)	C(60)–C(61)	1.60(4)
Rh(1)–C(73)	2.28(3)	C(61)–C(62)	1.48(4)
Rh(1)–C(74)	2.20(3)	C(62)–C(63)	1.54(4)
Rh(1)–Cg(69–70)[a]	2.14(2)	C(63)–C(64)	1.50(4)
Rh(1)–Cg(73–74)[a]	2.13(2)		
P(1)–Rh(1)–P(2)	82.4(3)	P(1)–Rh(1)–Cg(69–70)*	173.2(5)
P(2)–Rh(1)–Cg(73–74)*	169.1(5)	Cg(69–70)–Rh(1)–Cg(73–74)*	86.2(8)
P(1)–C(65)–C(66)–P(2)	50.8(18)	C(13)–C(14)–C(15)–C(16)	159(2)
P(1)–Rh(1)–P(2)–C(66)	4.8(9)	C(59)–C(60)–C(61)–C(62)	58(3)
Rh(1)–P(2)–C(66)–C(65)	−35.3(19)	C(60)–C(61)–C(62)–C(63)	166.2(18)
C(11)–C(12)–C(13)–C(14)	164.5(19)	C(61)–C(62)–C(63)–C(64)	56(3)
C(12)–C(13)–C(14)–C(15)	162(2)		

[a] Cg(x–y) denotes the center of gravity between C(x) and C(y).

ethanediyl bridged diphosphine complexes (83–87°),[12] but is similar to the natural bite angle calculated for dppe (81.7°).[13] Possibly, the difference in P–Rh–P bite-angle between CHIRAPHOS/DiPAMP and **1a** is due to the sterically more demanding environments in the bridge (CHIRAPHOS) or on the aryl ring (DiPAMP). The five-membered Rh–P–C–C–P chelate ring is close to an envelope conformation with C(65) lying out of the Rh–P–C–C–P least squares plane by 0.32(3) Å. It has been noted before that for [Rh(hfacac)(L_2)] (hfacac=[$CF_3C(O)CH$-$C(O)CF_3$]$^-$; L_2=ethanediyl-bridged diphosphine) no systematic preference for either a twist or an envelope conformation was found. Possibly, steric interactions and packing effects determine the ultimate conformation of the chelate ring.[14]

The C–C bond lengths in the COD ring are normal, except for C(73)–C(74) (1.41(4) Å) which is due to the rather poor quality of the diffraction data. As reported for [Rh(COD)-(CHIRAPHOS)]$^+$, the C=C double bonds of the COD-ring are not coordinated perpendicular to the P–Rh–P plane. This is also obvious from the angle between the planes defined by Cg(69–70)–Rh(1)–Cg(73–74) and P–Rh–P (13.1(8)°), which makes the environment around the Rh-atom distorted square planar. This also results in formation of two longer (Rh(1)–C(70), –C(73): 2.26(3) and 2.28(3) Å) and two shorter (Rh(1)–C(69), –C(74): 2.22(3) and 2.20(3) Å) Rh–C bonds, which can be explained by different steric hindrance exerted by the two aryl substituents of each phosphorus atom on the COD ligand.[12]

The four perfluoroalkyl tails can be divided in two sets. The three tails radiating away from Si(1), Si(2) and Si(3) show exclusive *trans* conformations along the carbon-skeleton with dihedral angles ranging from 159 to 170°, resulting in a helical (pig-tail) structure. The fourth tail radiating from Si(4), however, adopts a conformation with two dihedral angles (C(60)–C(61) and C(62)–C(63) are 58(3) and 56(3)°), which are typical for a *gauche* conformation. The remaining dihedral angles are all *trans* conformations.

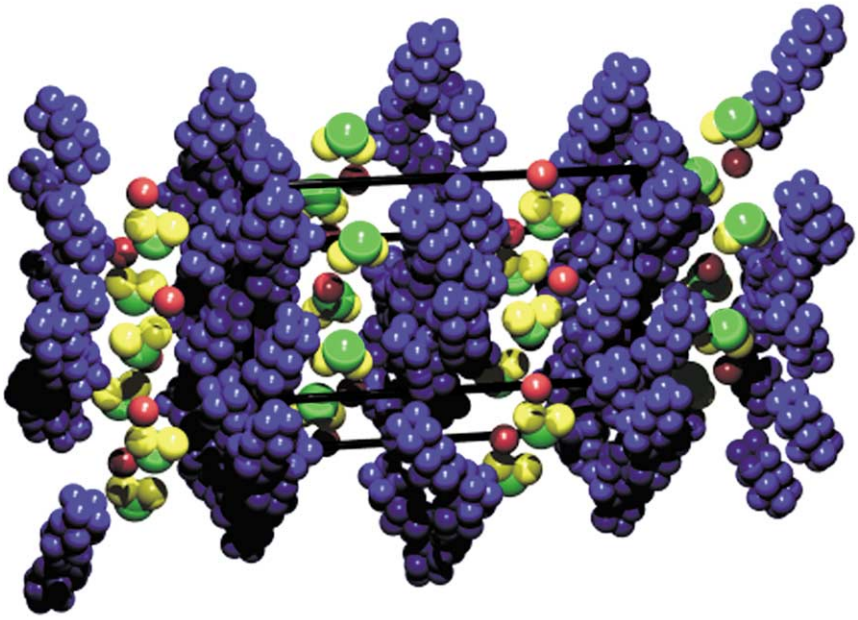

Figure 2. Packing diagram of **7** (F blue; P yellow; Rh green; B red; all other atoms are omitted for clarity).

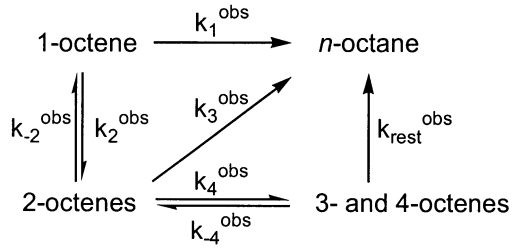

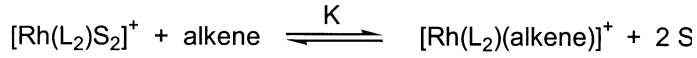

Scheme 1.

Indeed, the preferred conformation along the carbon chain in a perfluoroalkyl group in the solid state is *trans*.[15] However, different dihedral angles close to the alternative *gauche* conformations have also been observed in various crystal structures of transition metal complexes with fluorous ligands, the conformational changes most probably being induced by crystal packing effects.[11] The irregular C–C interatomic distances within the perfluoroalkyl groups are artifacts of the quality of the dataset.

The packing diagram of **7**, shown in Fig. 2, clearly shows the presence of fluorous and non-fluorous regions in the

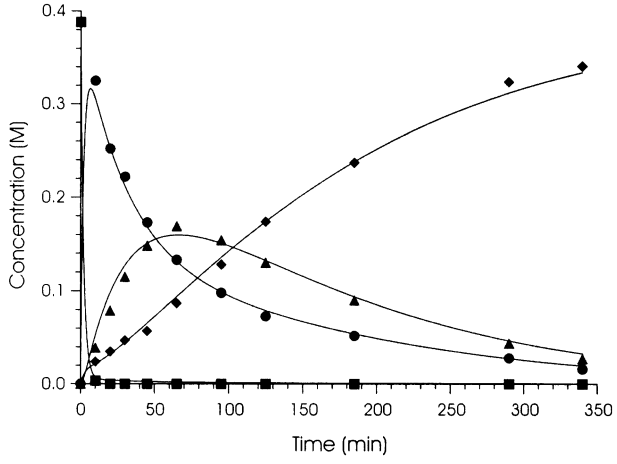

(a)

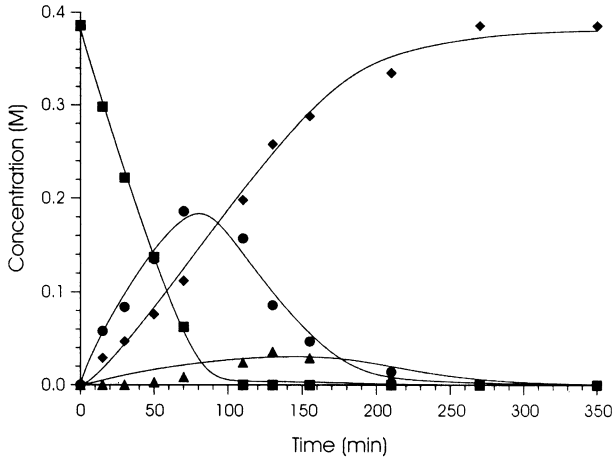

(b)

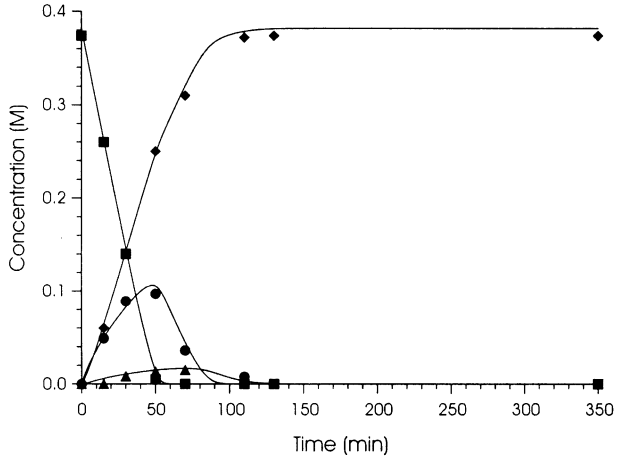

(c)

Figure 3. Conversion vs time plots of the hydrogenation of 1-octene using (a) [Rh(COD)(dppe)]BF_4, (b) **5** or (c) **4a**. (Legend: ■=1-octene; ●=2-octenes; ▲=3- and 4-octenes; ◆=*n*-octane; points are measured results from GC, solid line was fitted to the datapoints).

Table 3. Observed quantities and kinetic modeling of the hydrogenation of 1-octene

	[Rh(COD)(dppe)]BF_4	**5**	**6**	**4a**
para-Substituent	–H	$-SiMe_3$	$-SiMe_2(C_8H_{17})$	$-SiMe_2CH_2CH_2R_f$ $R_f=C_6F_{13}$
$TOF_{50\%}$[a]	9(2)	25(4)	25(4)	59(5)
cis/*trans* ratio[b]	0.29(1)	0.88(1)	0.87(1)	0.94(1)
Isomerization[c]	83(2)% (10 min)	59(2)% (65 min)	56(2)% (60 min)	31(2)% (45 min)
k_1^{obs} (min^{-1})	1.0(5)	0.10(7)	0.10(8)	0.6(2)
k_2^{obs} (min^{-1})	$7(2)\times10^1$	1.5(1)	1.7(2)	1.2(2)
k_{-2}^{obs} (min^{-1})	2(1)	0.20(1)	0.10(7)	0.2(1)
k_3^{obs} (min^{-1})	0.10(7)	0.5(1)	0.4(1)	0.6(4)
k_4^{obs} (min^{-1})	3(1)	0.20(8)	0.20(7)	0.2(1)
k_{-4}^{obs} (min^{-1})	1.3(7)	0.2(1)	0.10(6)	0.001(8)
k_{rest}^{obs} (min^{-1})	0.7(3)	0.10(6)	0.10(7)	0.3(1)
K (M^{-1})	2(1)	$3(2)\times10^1$	$3(2)\times10^1$	$8(2)\times10^1$

Conditions: T=40°C, $p(H_2)$=1 bar, stirring speed=1100 rpm, catalyst/1-octene=1:83, [Rh]=6 mM. For the definition of the parameters, see Scheme 1. All experiments were performed in duplo. Deviations are given in brackets.

[a] Turn-over frequency in mole *n*-octane/mole of Rh/hour determined when 50% of the maximum amount of *n*-octane was formed.

[b] Initial *cis*/*trans*-ratio of 2-octenes.

[c] Maximum amount of *cis*- and *trans*-2-octene; time given in brackets.

crystal lattice. The perfluoroalkyl parts of the molecules are assembled in separate layers. These layers are alternated with non-fluorous layers which contain the organic and charged parts of the molecules, i.e. this structure organizes the borate, rhodium and phosphorus containing parts of the molecules in single layers. This layered structure is clearly related to the amphiphilic character of **7** and represents a nice demonstration of the structural consequences of fluorous behavior in the solid state.

The hydrogenation of 1-octene in acetone as solvent served as a model reaction to study the consequences of silyl-functionalization on the catalytic reactivity by comparing the respective precatalysts [Rh(COD)(dppe)]BF_4, **4a**, **5** and **6** (Scheme 1). The resulting conversion vs time plots (Fig. 3) were fitted to a simplified kinetic model (see Section 4). The kinetic, catalytic and thermodynamic data thus obtained are represented in Table 3.

From inspection of these data it is clear that trimethylsilyl- (**5**) and dimethyloctylsilyl substitution (**6**) result in similar rate constants for hydrogenation but reduced isomerization rate constants (k_1^{obs} and k_3^{obs} relative to k_2^{obs} and k_4^{obs}) compared to parent [Rh(COD)(dppe)]BF_4. It can be concluded that **5** and **6** relative to [Rh(COD)(dppe)]BF_4 are more effective in hydrogenation because less alkene is first isomerized to internal alkene isomers that subsequently are more difficult to hydrogenate. Interestingly, both the *cis*-2-octene/*trans*-2-octene ratio after 15 min and the alkene association constant are increased for **5** and **6**.

Surprisingly, the effects observed upon trimethylsilyl- or dimethyloctylsilyl-substitution are even more pronounced upon 1*H*,1*H*,2*H*,2*H*-perfluoroalkyldimethylsilyl-functionalisation (**4a**), i.e. compared to **5** and **6**, the hydrogenation activity increased and the isomerization activity decreased. This is again accompanied by a higher initial *cis*/*trans* ratio for the 2-octene isomers formed, but also by a significantly higher alkene association constant *K*.

The large differences observed between the non-fluorous parent compound [Rh(COD)(dppe)]BF_4 and non-fluorous silyl-substituted **5** and **6**, and to an even higher extent fluorous **4a**, are difficult to explain in terms of electronic or steric effects. This is confirmed by the very similar ^{103}Rh NMR data of [Rh(COD)(dppe)]BF_4, **4a** and **5** and the analysis of the X-ray crystallographic structure of **7** (same fluorous cation as **4a**).

Stimulated by the crystallographic structure of **7**, which is clearly indicative of the tendency of this compound to aggregate, we wondered whether such 'fluorous self-assembly' could also be operative in solution. To obtain insight in the differences observed between [Rh(COD)(dppe)]BF_4, [Rh(COD)(**3**)]BF_4 (**6**) and [Rh(COD)(**1a**)]BF_4 (**4a**) in solution, 5 mM solutions in acetone were studied by dynamic light scattering (DLS). Since the results of direct deposit TEM (5–10 nm spheres) did not match the results obtained by DLS, the solutions were studied by cryo transmission electron microscopy (cryoTEM), where the sample is vitrified and kept in liquid nitrogen (Table 4 and Figs. 4 and 5). For *para*-dimethyloctylsilyl derivative **6**, the presence of aggregates was indeed established by both DLS and cryoTEM (Table 4). Similar and even larger structures were observed for **4a**. The sizes of the aggregates are within the typical range for vesicle-like structures.[16] Furthermore, the low transmission intensity in the center of the aggregates (Figs. 4 and 5) indicates that also the inside of the aggregates contains rhodium species, excluding a vacuole-like structure with a single bilayer and a solvent-containing interior. Surprisingly, small aggregates (30–50 nm) were even found for non-substituted [Rh(COD)(dppe)]BF_4 using DLS. However, this could not be confirmed by cryoTEM.

Table 4. Sizes of aggregates in 5 mM acetone solutions of derivatives of [Rh(COD)(dppe)]BF_4

Compound	cmc (mM)[a]	Radius (nm)	
		DLS	CryoTEM
[Rh(COD)(dppe)]BF_4	–	30–50	Not observed
4a	0.7	100–400	90–360
6	1.2	110–130	110–300

[a] Critical micelle concentration determined from conductivity measurements.

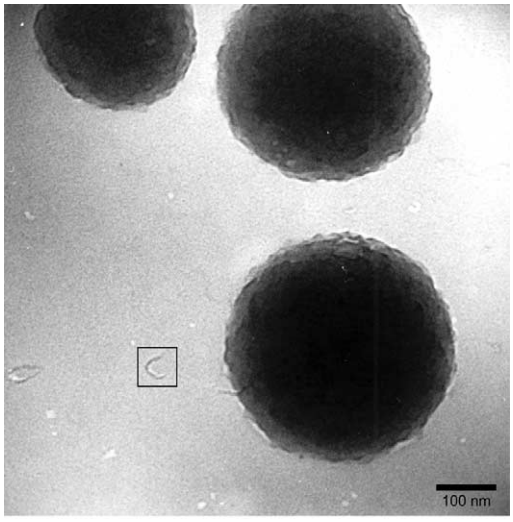

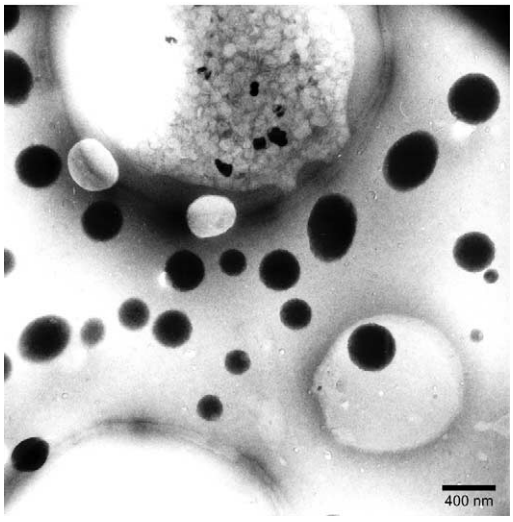

Figure 4. CryoTEM micrographs of 5 mM acetone solutions of **4a**.

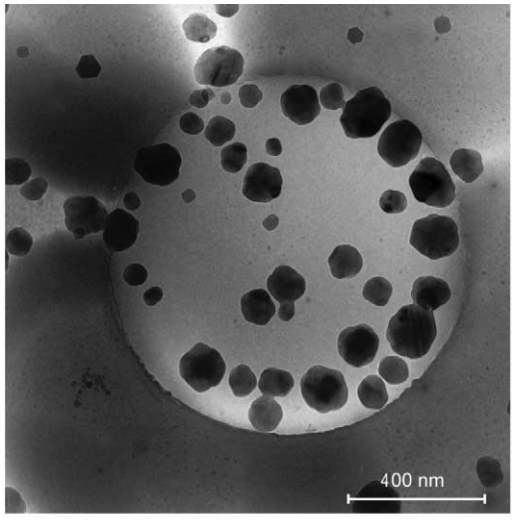

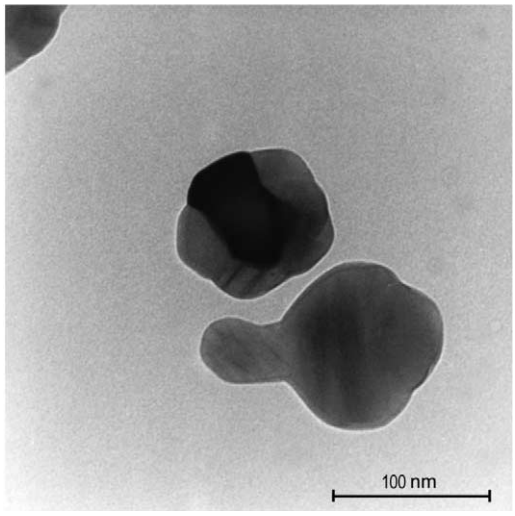

Figure 5. CryoTEM micrographs of 5 mM acetone solutions of **6**.

Furthermore, also some smaller, less well identifiable structures were observed for **4a** that were either free floating in solution or attached to the larger spheres. These structures (see Fig. 4, boxed area), are most likely bilayered segments, their cross diameter (ca. 4 nm) being in agreement with approximately twice the length of a 1*H*,1*H*,2*H*,2*H*-perfluorooctyl-moiety. Related bilayered, vesicle-like structures of fluorinated compounds in organic solvents were observed before for perfluoroalkyl diester derivatives of HOOC–CH(NHR)–$(CH_2)_2$COOH (R=alkyl or oligo glycol moiety) in cyclohexane.[17] It has been noted previously that the higher rigidity of perfluoroalkyl groups relative to normal alkyl groups, results in a smaller loss of entropy upon aggregation of the molecules containing these alkyl groups.[18] Consequently, compounds containing perfluoroalkyl groups have a higher tendency to aggregate than the corresponding non-fluorinated species. The irregular surface of the spheres in Fig. 4 might be due to an equilibrium between the fluorous rhodium species in the aggregate and freely dissolved in solution.

Critical micelle concentrations (cmc) of **4a** and **6** in acetone could be determined from conductivity measurements (Table 4), plotted as the equivalent conductance against the square root of the concentration (Fig. 6). For both compounds, the plot consists of two linear parts intersecting at a concentration which, following the interpretation of conductivity data in Ref. 19, can be identified as $(\text{cmc})^{1/2}$. The linear decrease in the molar conductivity Λ with $c^{1/2}$ observed above and below the cmc for both **4a** and **6**, is consistent with the behavior of strong electrolytes (the interactions between ions at higher concentrations retard their mobility[20]). The slope of the plot and consequently the extrapolated y intercept (Λ_0), is in both cases lower at concentrations above the cmc, indicating that the aggregated rhodium complex has a lower Λ_0. The molar conductivities above the cmcs are still considerable, indicating that the aggregates carry significant net charge. Interestingly, the cmc of fluorous **4a** is lower compared to the cmc of non-fluorous **6** (Table 4, Fig. 5). This is in agreement with the fluorous compound's higher tendency to aggregate.

The differences observed between the three types of catalysts ([Rh(COD)(dppe)]BF_4, non-fluorous silyl-substituted **5** and **6**, and fluorous **4a**) can be explained by the differences in aggregation behavior as described above. For aqueous systems, there is ample evidence in the literature to conclude that aggregation of homogeneous

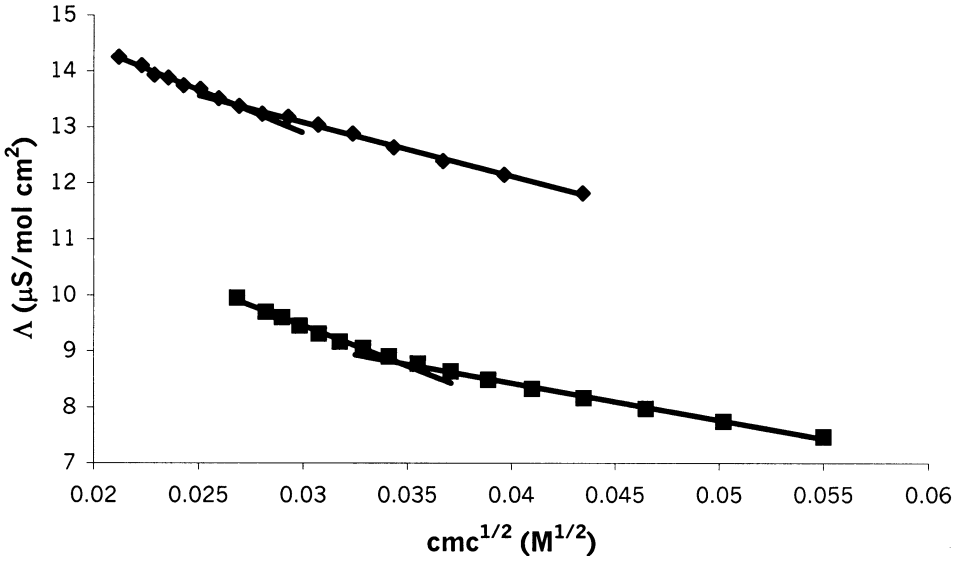

Figure 6. Conductivity measurements of acetone solutions of **4a** (◆) and **6** (■) for the determination of their critical micelle concentration.

catalysts can have beneficial effects on catalytic activity and/or selectivity.[21,22] Especially noteworthy are positive effects on enantioselectivity.[21,22] For aqueous emulsions containing micelle-forming surfactants, the solubility of apolar gasses (like CH_4, O_2, Ar, C_3H_8) can be 1.2 to 20 times higher compared to that in pure water.[23] This increased solubility of gaseous reactants could explain the positive effect of these surfactants on the catalytic activity in a number of cases.

In addition, the more lipophilic inside of an aggregate (lower dielectric constant) can cause a higher concentration of lipophilic substrate molecules as well as a lowered solvent concentration in the interior or vicinity of the aggregate compared to that of the bulk of the surrounding (more polar) solvent. Both effects can lead to an apparent higher association constant for a particular catalyst–substrate adduct. In our specific case, the rhodium complex is less well stabilized by solvent. Consequently, stabilization by association of substrate becomes more important, which leads to an apparently higher association constant K for the bulk of the reaction mixture.[16] Such modulation of substrate–catalyst interaction appears to be a quite general phenomenon in metalloaggregates.[16] However, it should be noted that, since the association constant K is an average for all alkenes present in the bulk of the reaction mixture and *trans*-alkenes compared to *cis*- and primary alkenes have in general a lower tendency to complex to metals,[24] the higher association constant found for **4a**, **5** and **6** relative to [Rh(COD)(dppe)]BF_4 could be partly due to the lower proportion of internal *trans*-alkenes formed.

When translated to the case of an aggregated catalyst in a polar but organic acetone solution, it can be argued that the higher catalytic activity observed for non-fluorous **5** and **6** and fluorous **4a** is caused by the combined effects of a locally increased dihydrogen concentration and an aggregate-induced higher affinity of the catalyst for the alkene substrate. The latter effect appears to be the dominant one (Table 3). The larger size and more apolar environment of the fluorous aggregates of **4a** (relative to **5** and **6**), possibly result in the more pronounced difference in catalytic performance relative to reference compound [Rh(COD)-(dppe)]BF_4.

Except for the positive effects on the hydrogenation rate constants and the higher K, alkene isomerization (k_2), which most likely involves allylic C–H activation of the alkene,[25] appears to be disfavoured in the (fluorous) aggregates. In general, the nature of the effect responsible for different (enantio)selectivities in micellular environments remains unclear and it is also not immediately obvious why isomerization should be more difficult in an aggregate.[21,22]

The difference in initial *cis*/*trans*-2-octene ratio observed between the (fluorous) silyl-substituted catalysts (0.87–0.94) and reference catalyst [Rh(COD)(dppe)]BF_4 (0.29) could be explained by the higher isomerization activity of the latter. A thermodynamic 1:3 *cis*/*trans*-2-octene mixture was observed for [Rh(COD)(dppe)]BF_4, while the kinetically 1:1 mixture, as predicted by the π-allyl mechanism,[25] was detected for the silyl-substituted catalysts with lower isomerization activity.

To further explore the impact of aggregation on the catalytic selectivity, the semi-hydrogenation of 4-octyne was studied (Scheme 2). For all catalysts tested, 4-octyne was converted with moderate selectivity to *cis*-4-octene, which was subsequently hydrogenated to *n*-octane or first isomerized to other internal alkenes and then hydrogenated. Similar behavior had been observed previously for the hydrogenation of 2-hexyne by [Rh(nbd)(dppe)]BF_4.[26] Activities and maximum selectivities towards *cis*-4-octene for different catalytic systems are given in Table 5. Much like the observations described above for the hydrogenation of 1-octene, the hydrogenation activity increased upon trimethylsilyl-functionalization and increased even further upon attachment of dimethyl(1*H*,1*H*,2*H*,2*H*-perfluorooctyl)silyl-groups. The higher hydrogenation activity may explain the relatively higher proportion of overhydrogenation to *n*-octane and a consequently lower selectivity

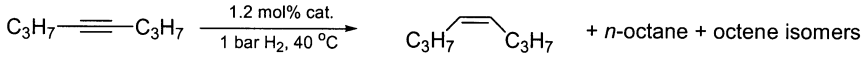

Scheme 2.

towards *cis*-4-octene for the functionalized catalysts. As observed for the hydrogenation of 1-octene, the fluorous catalysts again produced lower amounts of isomerization products. A further increase of the number of perfluoroalkyl groups to 8 (**4b**) resulted in a lower hydrogenation activity but similar maximum selectivity compared to **4a**.

Different solvent systems were needed to perform hydrogenations using the highly fluorous complex **4c**. Since it is known that the solvent influences the catalytic activity, no direct conclusions regarding the effect of perfluoroalkyl-functionalization by comparison with the activities and selectivities of **4a**,**b**, **5** and [Rh(cod)(dppe)]BF_4 can be drawn. Three types of solvent system were considered: a biphasic combination of a non-coordinating fluorous solvent (PFMCH) and a coordinating organic solvent (acetone), a biphasic combination of a potentially coordinating, fluorous solvent (FC-75) and a non-coordinating, organic solvent (hexanes) and finally a monophasic combination also consisting of hexanes and FC-75 but in a 1:3 volumetric ratio. Using acetone as the organic phase, the hydrogenation activity of **4c** was, despite the biphasic nature of the solvent system, comparable to the activity of **4b** in pure acetone. With apolar hexane as the organic solvent, the observed activity was lower than that observed using acetone. Furthermore, the monophasic version of this reaction medium resulted in higher activity than the biphasic system, possibly due to the absence of mass transfer limitations. It should also be noted that under the nearly homogeneous conditions, **4c** displayed comparable activity to non-fluorous [Rh(COD)(dppe)]BF_4 and a similar maximum selectivity compared to **4a**.

Recycling experiments using **4c** were performed in PFMCH/acetone (1:1) or FC-75/hexane (1:3) as solvent systems (Table 6). The higher activity of **4c** in PFMCH/acetone is reflected in the higher conversions obtained after 2.5 h. In both systems, the catalyst can be efficiently recycled, since no significant drops in conversions are observed and in PFMCH/acetone even a small increase of the conversion was found. Leaching of both rhodium and phosphorus was higher for the system containing acetone in contrast to the very low leaching values obtained when hexane was used as organic layer. For PFMCH/acetone the amount of Rh and P found in the organic layer corresponded to a 1:2 molar ratio, indicating that leaching of the intact catalyst and not of free ligand occurred. This shows that the use of bidentate diphosphines solves the problem of ligand-leaching, which was encountered previously for monodentate phosphines in Wilkinson-type catalysts.[27] For FC-75/hexane, a small excess of phosphorus was found in the organic layer, most likely indicating that some catalyst had decomposed as no rhodium was found. The amount of leaching of the fluorous solvent into the organic layer, which is a known issue in fluorous biphasic catalysis, was ca. 20% per cycle for FC-75/hexane but was not observed for PFMCH/acetone due to their low miscibility.

3. Conclusions

Fluorous diphosphines **1a–c** and silyl-substituted, non-fluorous diphosphines **2** and **3** were used for the synthesis of fluorous and non-fluorous rhodium complexes. The latter were shown to be active in the hydrogenation of 1-octene and 4-octyne.

Important differences were observed in the catalytic performance of the three types of catalyst, i.e. fluorous catalysts **4a–c**, non-fluorous silyl substituted catalyst **5–6** and [Rh(COD)(dppe)]BF_4. Formation of aggregates, confirmed by DLS and cryoTEM for [Rh(COD)(**1a**)]BF_4 (**4a**) and [Rh(COD)(**3**)]BF_4 (**6**) are most likely responsible for the lower isomerization activities and higher alkene-associations constants observed for silyl-substituted, non-fluorous catalysts **5** and **6**. The similar but more pronounced effects observed for fluorous catalysts **4** in acetone, possibly due to the larger size of the aggregates and/or a higher degree of ordering, can be explained in this way as well.

Table 5. Results of hydrogenation of 4-octyne (conditions: T=40°C, $p(H_2)$=1 bar, stirring speed=1100 rpm, catalyst/4-octyne=1:83, catalyst loading: 6 μmol per mL of reaction volume) using parent compound [Rh(COD)(dppe)]BF_4, **4a–c** or **5**

Catalyst precursor	Solvent system[a]		TOF[b]	Max. selectivity[c]	Max. isomers[d]
[Rh(COD)(dppe)]BF_4	Me_2CO	1	32	83 (185 min)	31 (240 min)
5	Me_2CO	1	43	74 (105 min)	29 (180 min)
4a	Me_2CO	1	77	70 (75 min)	18 (115 min)
4b	Me_2CO	1	36	67 (115 min)	16 (165 min)
4c	PFMCH/Me_2CO (1:1)	2	31	61 (185 min)	15 (295 min)
4c	FC-75/*n*-hexane (1:1)	2	12	70 (310 min)	17 (340 min)[e]
4c	FC-75/*n*-hexane (1:3)	1[f]	23	68 (205 min)	17 (295 min)

[a] Solvents and number of liquid phases are given. Volume ratios are given in brackets
[b] TOF=turn over frequency in mole of substrate/mol of Rh/hour at 50% conversion.
[c] Towards *cis*-4-octene.
[d] Maximum amount of isomerization products of *cis*-4-octene, time given in brackets.
[e] The reaction was not complete after 340 min.
[f] Most of the catalyst is emulsified in the otherwise homogeneous reaction mixture.

Table 6. Recycling and reuse of **4c** in 4-octyne hydrogenation for two fluorous (biphasic) solvent systems

Cycle	Conversion after 2.5 h (%)	
	PFMCH/acetone (1:1)	FC-75/hexane (1:3)
1	89	59
2	93	63
3	94	57
Rh-leaching[a]	2.5% (36 ppm)	<0.08% (<1 ppm)[b]
P-leaching[a]	2.2% (19 ppm)	0.4% (3 ppm)

For conditions, see Table 5. Phase separation was performed at 0°C.
[a] Determined by ICP-AAS analysis of the organic layer of the first cycle.
[b] Below the detection limit (1 ppm).

It may be clear that formation of aggregates of 'light fluorous'[28] catalyst molecules in polar organic solvents opens up a new and interesting field for application of fluorous catalysts in homogeneous catalysis.

Furthermore, we have demonstrated that highly fluorous rhodium catalyst **4c** can be efficiently recycled in two different fluorous biphasic systems, resulting in 2.5% (for PFMCH/acetone) and <0.08% (for FC-75/hexane) leaching of rhodium. It is important to note that the use of diphosphines solves the problem of dissociation and leaching of free ligand, which was observed for catalytic systems containing monophosphines.

4. Experimental

4.1. General

All experiments were performed in a dry dinitrogen atmosphere using standard Schlenk techniques. Solvents were stored over sodium benzophenone ketyl or CaH_2 and were distilled before use. Fluorinated solvents (c-$CF_3C_6F_{11}$ (Lancaster), FC-72 and $CF_3C_6H_5$ (Acros)) were degassed and stored under dinitrogen atmosphere. Derivatives of dppe (**1**–**2**),[7] [Rh(COD)(dppe)]BF_4,[8] [Rh(acac)(COD)],[29] [Rh(COD)$_2$]BF_4[30] and 1,2-bis[bis(*p*-bromophenyl)phosphino]ethane[7] were prepared according to previously reported procedures. Other chemicals were obtained from commercial suppliers (Acros, Aldrich, Lancaster) and used as delivered. Microanalyses were carried out by H. Kolbe, Mikroanalytisches Laboratorium, Mülheim an der Ruhr. ^{19}F NMR spectra were externally referenced against $CFCl_3$ (δ=0 ppm) and ^{31}P NMR spectra were referenced against H_3PO_4 (δ=0 ppm).

4.2. DLS measurements

Solutions were filtered through a P4 filter (pore size=10–16 μm). Dynamic light scattering (DLS) results were obtained using an argon ion laser (Spectra Physics Series 2000) operating at 514.5 nm. Auto correlation functions were measured with a Malvern Multibit K7025 128 points correlator. Diffusion coefficients D_0 were obtained from a second order cumulant fit using auto correlation functions obtained from angles between 35 and 120°. If a single exponential fit of the autocorrelation function could not be obtained, possibly due to polydispersity, the diffusion coefficient was estimated from 5τ (τ=half time). The hydrodynamic radius, R_h, was calculated using the Stokes–Einstein relation, $D_0 = kT/6\pi\eta R_h$, in which kT is the thermal energy and η the solvent viscosity.

4.3. CryoTEM measurements

Specimen preparation and vitrification was done with a Vitrobot (see http://www.maastrichtinstruments.nl/projects/vr/index.html). Quantifoil grids (200 mesh copper grids R 2/2, Quantifoil Micro Tools GmbH, Jena, Germany) were used for sample preparation. In the chamber of the Vitrobot, 3 μL of the sample was applied to the grid, the grid was blotted twice (each blotting action lasted 2 s) and shot in liquid nitrogen for vitrification. Liquid ethane, an efficient coolant for aqueous solutions/suspensions, was found incompatible with the solvent used (40% acetone); apparently the vitrified material dissolved in liquid ethane. Liquid nitrogen, with a much slower heat exchange than liquid ethane, proved to be inert and despite poor heat exchange the solvent matrix was vitrified under the experimental conditions. After preparation of a vitrified thin film on a quantifoil grid, the grid was mounted in a cryo-holder (Gatan 626) and transferred to a Philips CM 12 transmission microscope for observation at −170°C and 120 kV. Low dose conditions were used to take micrographs to ensure that the area of interest had minimal beam exposure before micrographs were taken.

4.4. X-Ray structure determination of 7

X-ray data were collected on a Nonius TurboCAD4 diffractometer (Rotating anode, Mo Kα, λ=0.71073 Å, T=150 K, θ_{max}=21.5°) for a yellowish plate shaped crystal (0.5×0.5×0.05 mm^3) glued with perfluor oil on top of a Lindemann glass capillary. The crystal was found to diffract poorly at higher diffraction angles and with structured reflection profiles, resulting in data of limited quality, though sufficient for the purpose of this study. The structure was solved with Patterson techniques and completed with difference Fourier syntheses. Correction for absorption was deemed unnecessary. Hydrogen atoms were included at calculated positions. Full matrix least squares refinement on F^2 (SHELXL-97[31]) converged at R=0.15 ($wR2$=0.37, S=1.05, 676 parameters, 12410 reflections, max and min residual density 0.88 and −0.66 e Å^{-3}). Rhodium and silicon were refined with anisotropic parameters, all other non-hydrogen atoms with isotropic displacement parameters. Geometrical calculations and the ORTEP illustration were done with PLATON.[32] Pertinent data: monoclinic, space group $P_{2_1/c}$, Z=4, **a**=14.8704(13) Å, **b**=41.044(4) Å, **c**=22.691(2) Å, β=128.523(7)° $C_{74}H_{72}F_{52}P_2RhSi_4.C_{24}H_{20}B$, MW=2545.74, D_x=1.5606 g cm^{-3}, μ(Mo Kα) 0.37 mm^{-1}. Full details have been deposited with the Cambridge Crystallographic Data Centre (CCDC 172832).

4.4.1. 1,2-Bis[bis{4-((dimethyloctyl)silyl)phenyl}phosphino]ethane (3). A solution of 0.74 g 1,2-bis[bis(*p*-bromophenyl)phosphino]ethane (1.04 mmol) in THF (20 mL) was cooled to −90°C and 5.5 mL of a solution of *t*-BuLi (1.5 M; 8.3 mmol) was added. After stirring for 30 min while keep-

ing the temperature lower than −60°C, 0.86 g (4.15 mmol) of $C_8H_{17}SiMe_2Cl$ was added. After heating to room temperature, all volatiles were evaporated. The residue was dissolved in CH_2Cl_2/degassed water. The organic layer was separated, dried on $MgSO_4$ and evaporated to dryness, yielding 1.04 g (93%) of a clear light brown oil. Anal. calcd for $C_{66}H_{112}P_2Si_4$: C 73.41, H 10.45; Found: C 69.67, H 10.93; ^{1}H NMR (200 MHz, $CDCl_3$): δ 0.28 (s, 24H), 0.77 (m, 8H), 0.92 (t, $^3J_{HH}$=3.4 Hz, 12H), 1.29 (m, 48H), 2.16 (ps t, J=3.5 Hz, 4H), 7.35–7.54 (m, 16H); ^{31}P NMR ($CDCl_3$, 81.0 MHz): δ −12.0.

4.4.2. [Rh(COD)(1a)]BF_4 (4a). Compound **1a** (0.76 g; 0.38 mmol) dissolved in CH_2Cl_2 (30 mL) was added to a solution of [Rh(COD)$_2$]BF_4 (153 mg; 0.38 mmol) in CH_2Cl_2 (10 mL). After stirring for 10 min and evaporating all solvent in vacuo, the residue was washed with benzene. Drying of the precipitate yielded 0.62 g (70%) of an orange solid. Anal. calcd for $C_{74}H_{72}BF_{56}P_2RhSi_4$: C 38.42, H 3.14, P 2.68; Found: C 38.49, H 3.20, P 2.48; ^{1}H NMR (200 MHz, $CDCl_3$): δ 0.39 (s, 24H), 1.03 (m, 8H), 1.91–2.42 (m, 20H), 4.94 (m, 4H), 7.64 (m, 16H); ^{19}F NMR (282.4 MHz, $CDCl_3$): δ −154.0 (m, 4F), −126.6 (m, 8F), −123.6 (m, 8F), −123.4 (m, 8F), −122.5 (m, 8F), −116.3 (m, 8F), −81.3 (m, 12F).

4.4.3. [Rh(COD)(1b)]BF_4 (4b). Compound **1b** (3.24 g; 0.97 mmol) dissolved in $CF_3C_6H_5$ (15 mL) was added to a solution of [Rh(COD)$_2$]BF_4 (393 mg; 0.97 mmol) in CH_2Cl_2 (10 mL). After evaporation of all volatiles, the crude oil was dissolved in a biphasic system consisting of CH_2Cl_2 (10 mL) and PFMCH (25 mL). Phase separation and drying of the fluorous layer gave 3.36 g of an orange to red oil (95%). Anal calcd for $C_{102}H_{76}BF_{108}P_2RhSi_4$: C 33.64, H 2.10, P 1.70, F 56.34; Found: C 33.46, H 1.96, P 1.63, F 56.28; ^{1}H NMR (200 MHz, C_6D_6/FC-72, 1:1 v/v): δ 0.12 (br, 12H), 0.85 (br, 16H), 1.5–2.6 (br, 28H), 4.86 (br, 4H), 7.57 (br, 16H); ^{19}F NMR (282.4 MHz, $CDCl_3$/$CF_3C_6H_5$, 1:1 v/v): δ −152.2 (m, 4F), −126.9 (m, 16F), −123.8 (m, 16F), −123.5 (m, 16F), −122.5 (m, 16F), −116.4 (m, 16F), −81.8 (m, 24F).

4.4.4. [Rh(COD)(1c)]BF_4 (4c). Compound **1c** (1.57 g; 0.336 mmol) dissolved in PFMCH (10 mL) was added to a solution of [Rh(COD)$_2$]BF_4 (136 mg; 0.336 mmol) in CH_2Cl_2 (15 mL), while stirring vigorously (1500 rpm). Phase separation and evaporation to dryness yielded 1.66 g of an orange to red oil (99%). Anal. calcd for $C_{130}H_{80}BF_{160}P_2RhSi_4$: C 31.42, H 1.62, P 1.25; Found: C 31.32, H 1.56, P 1.31; ^{1}H NMR (200 MHz, C_6D_6/FC-72, 1:1 v/v): δ 1.08 (br, 24H), 1.96 (br, 36H), 4.79 (br, 4H), 7.57 (br, 16H).

4.4.5. [Rh(COD)(2)]BF_4 (5). Compound **2** (0.23 g; 0.32 mmol) dissolved in CH_2Cl_2 (20 mL) was added to a solution of [Rh(COD)$_2$]BF_4 (131 mg; 0.32 mmol) in CH_2Cl_2 (5 mL). Removal of all volatiles, washing with pentane and drying in vacuo yielded 0.31 g of an orange solid (96%). Anal. calcd for $C_{46}H_{68}BF_4P_2RhSi_4$: C 56.09, H 6.96; Found: C 53.73, H 6.68; ^{1}H NMR (200 MHz, $CDCl_3$): δ 0.32 (s, 24H), 2.31 (m, 12H), 4.96 (br, 4H), 7.61 (m, 16H); ^{19}F NMR (282.4 MHz, $CDCl_3$): δ −154.0 (m, 4F).

4.4.6. [Rh(COD)(3)]BF_4 (6). Compound **3** (0.14 g; 0.13 mmol) dissolved in CH_2Cl_2 (20 mL) was added to a solution of [Rh(COD)$_2$]BF_4 (53 mg; 0.13 mmol) in CH_2Cl_2 (10 mL). After stirring for 30 min, all volatiles were removed in vacuo and the product, 0.17 g (95%) of a red oil, was not purified any further. Anal. calcd for $C_{74}H_{124}BF_4P_2RhSi_4$: C 64.51, H 9.07; Found: C 61.59, H 8.14; ^{1}H NMR (200 MHz, $CDCl_3$): δ 0.31 (s, 24H), 0.86 (m, 20H), 1.26 (m, 48H), 2.2–2.6 (m, 12H), 4.95 (br, 4H), 7.60 (m, 16H).

4.4.7. [Rh(COD)(1a)]BPh_4 (7). Compound **1a** (0.82 g; 0.41 mmol) dissolved in THF (15 mL) was added to a solution containing [Rh(acac)(COD)] (128 mg; 0.41 mmol) and $NaBPh_4$ (0.28 g; 0.82 mmol). After stirring for 10 min and evaporating all volatiles in vacuo, CH_2Cl_2 (10 mL) was added. After filtration and drying, 0.76 g (73%) of an orange solid was obtained. Crystals suitable for X-ray structure analysis were grown from CH_2Cl_2/hexane. Anal. calcd for $C_{98}H_{92}BF_{52}P_2RhSi_4$: C 46.43, H 3.66, P 2.44; Found: C 46.05, H 3.70, P 2.62; ^{1}H NMR (200 MHz, $CDCl_3$): δ 0.38 (s, 24H), 1.02 (m, 8H), 2.10 (m, 20H), 4.93 (m, 4H), 6.76 (m, 4H), 6.86 (m, 8H), 7.30 (m, 8H), 7.44 (m, 8H), 7.60 (m, 8H); ^{31}P NMR ($CDCl_3$, 81.0 MHz): δ 56.1 ($^1J_{RhP}$=148.4 Hz).

4.5. Catalytic reactions and recycling

Three hydrogenation reactions were performed simultaneously in a Micronic 12 Place Heated Carousel Reaction Station. In a typical experiment, 36 μmol of catalyst was dissolved in 6 mL of the appropriate solvent or solvent mixture. The inert nitrogen atmosphere was replaced by hydrogen and the mixture was stirred at 1100 rpm at 40°C for 1 h.[33] Subsequently, substrate (0.44 mL) and *n*-decane (0.40 mL, internal standard) were added. Samples taken at regular time intervals were analyzed by GC. In recycling experiments, the reaction mixture was cooled to 0°C after 2.5 h while stirring was stopped and the hydrogen atmosphere was maintained. The organic layer was removed and new substrate and *n*-decane were added. Subsequently, the reaction mixture was heated to 40°C and a new cycle was started.

4.6. Kinetic model for $[Rh(L_2)]^+$-catalyzed hydrogenation (L_2=chelating ligand) and kinetic fitting

The rate equation for each step x in Scheme 1 (x=1, 2, −2, 3, 4, −4, rest) can be defined as:[34]

$$r_x = \frac{k_x^{obs} K[\mathrm{Rh}]_{tot}[\mathrm{alkene}]}{1 + K[\mathrm{alkene}]}$$

which corresponds to the mechanistic pathways depicted in Scheme 3. $[Rh]_{tot}$ is the total concentration of all rhodium species in solution, [alkene] is the concentration of the respective alkene involved in each step x and k_x^{obs} is the observed rate constant for step x.

The (constant) hydrogen pressure (total pressure kept at 1 bar) is included in k_x^{obs} of the hydrogenation steps (x=1, 3 or rest). In this model, it is assumed for simplicity that all alkenes have an average association constant K. Furthermore, no distinction between *cis*- and *trans*-alkenes was

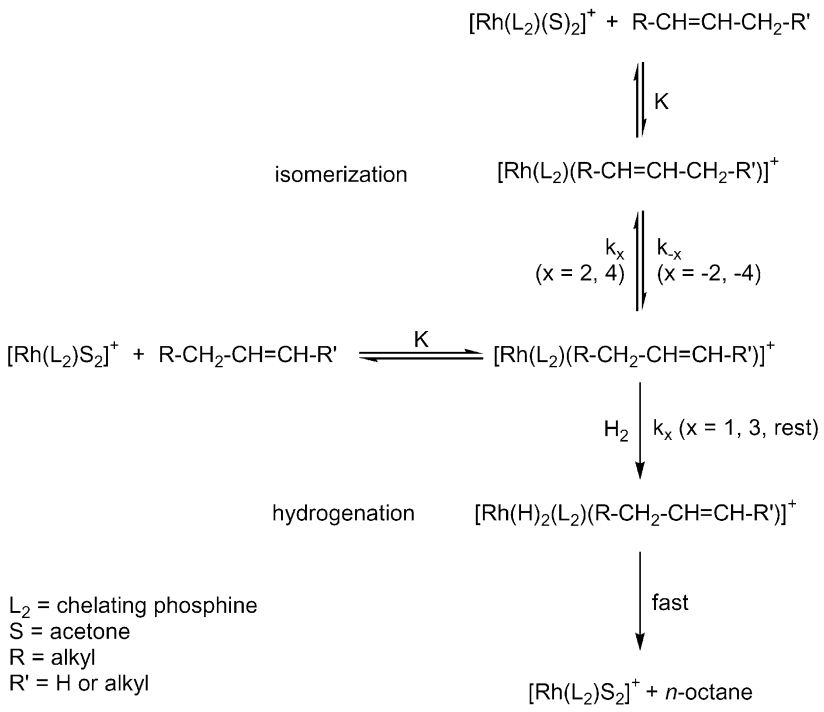

Scheme 3.

made. For $[RH(COD)(dppe)]BF_4$, Winstein–Holness kinetics[35] were applied to the 3- and 4-octene hydrogenation steps by defining one overall rate constant (k^{obs}_{rest}). In the case of catalysts **4a**, **5** and **6**, no significant amount of 4-octenes was observed.

Conversion vs time plots were fitted, using the program Micromath Scientist for Windows, version 2.0, to the model as shown in Scheme 1. Fitting was proceeded until the squared difference between measured and calculated concentrations was lower than 0.005.

Acknowledgements

ATOFINA Vlissingen B. V., NWO(ALS) and the Dutch Ministry of Economic Affairs (SENTER/BTS) are gratefully thanked for the financial support. Ing. J. M. Ernsting (University of Amsterdam) is thanked for the ^{103}Rh NMR measurements.

References

1. See for example: Brunner, H. In *Applied Homogeneous Catalysis with Organometallic Compounds*, Cornils, B., Herrmann, W. A., Eds.; VCH: Weinheim, 1996; p. 201 Chapter 2.2.
2. (a) de Wolf, E.; van Koten, G.; Deelman, B.-J. *Chem. Soc. Rev.* **1999**, *28*, 37. (b) Hope, E. G.; Stuart, A. M. *J. Fluorine Chem.* **1999**, *100*, 75. (c) Cavazzini, M.; Montanari, F.; Pozzi, G.; Quici, S. *J. Fluorine Chem.* **1999**, *94*, 183. (d) Rutherford, D.; Juliette, J. J. J.; Rocaboy, C.; Horváth, I. T.; Gladysz, J. A. *Catal. Today* **1998**, *42*, 381. (e) Horváth, I. T. *Acc. Chem. Res.* **1998**, *31*, 641. (f) Curran, D. P. *Angew. Chem., Int. Ed. Engl.* **1998**, *37*, 1174. (g) Cornils, B. *Angew. Chem., Int. Ed. Engl.* **1997**, *36*, 2057.
3. (a) Hope, E. G.; Kemmitt, R. D. W.; Stuart, A. M. *J. Chem. Soc., Dalton Trans.* **1998**, 3765. (b) Kainz, S.; Koch, D.; Baumann, W.; Leitner, W. *Angew. Chem., Int. Ed. Engl.* **1997**, *36*, 1628.
4. Hope, E. G.; Kemmitt, R. D. W.; Paige, D. R.; Stuart, A. M. *J. Fluorine Chem.* **1999**, *99*, 197.
5. (a) Klement, I.; Lütjens, H.; Knochel, P. *Angew. Chem., Int. Ed. Engl.* **1997**, *36*, 1454. (b) Haar, C. M.; Huang, J.; Nolan, S.; Petersen, J. L. *Organometallics* **1998**, *17*, 5018.
6. (a) Kleijn, H.; Jastrzebski, J. T. B. H.; Gossage, R. A.; Kooijman, H.; Spek, A. L.; van Koten, G. *Tetrahedron* **1998**, *54*, 1145. (b) Richter, B.; de Wolf, E.; van Koten, G.; Deelman, B.-J. *J. Org. Chem.* **2000**, *65*, 3885.
7. de Wolf, E.; Richter, B.; Deelman, B.-J.; van Koten, G. *J. Org. Chem.* **2000**, *65*, 5424.
8. Schrock, R. R.; Osborn, J. A. *J. Am. Chem. Soc.* **1971**, *93*, 2397.
9. No significant changes in line broadening were observed upon heating to 50°C.
10. Leitner, W.; Bühl, M.; Fornika, R.; Six, C.; Baumann, W.; Dinjus, E.; Kessler, M.; Krüger, C.; Rufinska, A. *Organometallics* **1999**, *18*, 1196.
11. (a) Bhattacharyya, P.; Croxtall, B.; Fawcett, J.; Fawcett, J.; Gudmunsen, D.; Hope, E. G.; Kemmitt, R. D. W.; Paige, D. R.; Russell, D. R.; Stuart, A. M.; Wood, D. R. W. *J. Fluorine Chem.* **2000**, *101*, 247. (b) Fawcett, J.; Hope, E. G.; Kemmitt, R. D. W.; Paige, D. R.; Russell, D. R.; Stuart, A. M. *J. Chem. Soc., Dalton Trans.* **1998**, 3751. (c) Guillevic, M. A.; Arif, A. M.; Horváth, I. T.; Gladysz, J. A. *Angew. Chem., Int. Ed. Engl.* **1997**, *36*, 1612. (d) Fawcett, J.; Hope, E. G.; Kemmitt, R. D. W.; Paige, D. R.; Russell, D. R.; Stuart, A. M.; Cole-Hamilton, D. J.; Payne, M. J. *Chem. Commun.* **1997**, 1127. (e) Guillevic, M. A.; Rocaboy, C.; Arif, A. M.; Horváth, I. T.; Gladysz, J. A. *Organometallics* **1998**, *17*, 707.

12. Burk, M. J.; Feaster, J. E.; Nugent, W. A.; Harlow, R. L. *J. Am. Chem. Soc.* **1993**, *115*, 10125. (b) Giovanetti, J. S.; Kelly, C. M.; Landis, C. R. *J. Am. Chem. Soc.* **1993**, *115*, 4040. (c) Ball, R. G.; Payne, N. C. *Inorg. Chem.* **1977**, *16*, 1187.
13. Casey, C. P.; Whiteker, G. T. *Isr. J. Chem.* **1990**, *30*, 299.
14. Angermund, K.; Baumann, W.; Dinjus, E.; Fornika, R.; Görls, H.; Kessler, M.; Krüger, C.; Leitner, W.; Lutz, F. *Chem. Eur. J.* **1997**, *3*, 755.
15. Bunn, C. W.; Howells, E. R. *Nature* **1954**, *174*, 549.
16. Scrimin, P. In *Supramolecular Control of Structure and Reactivity*, Hamilton, A. D., Ed.; *Perspectives in Supramolecular Chemistry*; Wiley: Chichester, 1996; Vol. 3, p. 101.
17. Ishikawa, Y.; Kuwahara, H.; Kunitake, T. *J. Am. Chem. Soc.* **1989**, *111*, 8530.
18. (a) Wang, K.; Karlsson, G.; Almgren, M.; Asakawa, T. *J. Phys. Chem.* **1999**, *103*, 9237. (b) Blokzijl, W.; Engberts, J. B. F. N. *Angew. Chem., Int. Ed. Engl.* **1993**, *32*, 1545.
19. Guo, W.; Brown, T. A.; Fung, B. M. *J. Phys. Chem.* **1991**, *95*, 1829.
20. The molar conductivity Λ is defined as $\Lambda=\Lambda_0-Sc^{1/2}$ where S is linearly dependant on the molar conductivity at infinite dilution (Λ_0). Fernandez-Prini, R. In *Physical Chemistry of Organic Solvent Systems*, Covington, A. K., Dickinson, T., Eds.; Plenum: London, 1973 Chapter 5.
21. (a) Grassert, I.; Oehme, G. *J. Organomet. Chem.* **2001**, *621*, 158. (b) Grassert, I.; Schmidt, U.; Ziegler, S.; Fischer, C.; Oehme, G. *Tetrahedron: Asymmetry* **1998**, *9*, 4193. (c) Selke, R.; Holtz, J.; Riepe, A.; Börner, A. *Chem. Eur. J.* **1998**, *4*, 769. (d) Yonehara, K.; Ohe, K.; Uemara, S. *J. Org. Chem.* **1999**, *64*, 9381. (e) Goedheijt, M. S.; Hanson, B. E.; Reek, J. N. H.; Kamer, P. C. J.; van Leeuwen, P. W. N. M. *J. Am. Chem. Soc.* **2000**, *122*, 1650. (f) Hanson, B. E.; Ding, H.; Kohlpainter, C. W. *Catal. Today* **1998**, *42*, 421. (g) Ding, H.; Hanson, B. E.; Bartik, T.; Bartik, B. *Organometallics* **1994**, *13*, 3761.
22. For reviews on micellar catalysis, see: (a) Oehme, G.; Grassert, I.; Paetzold, E.; Meisel, R.; Drexler, K.; Fuhrmann, H. *Coord. Chem. Rev.* **1999**, *185–186*, 585. (b) Oehme, G. In *Aqueous-Phase Organometallic Catalysis, Concepts and Applications*, Cornils, B., Herrmann, W. A., Eds.; Wiley-VCH: Weinheim, 1999; p. 193.
23. (a) Hai, M.; Han, B.; Yan, H.; Han, Q. *Phys. Chem. Chem. Phys.* **1999**, *1*, 445. (b) Radwan, N.; King, Jr., A. D. *J. Colloid Interf. Sci.* **1997**, *194*, 120. (c) Roy, S.; Mehra, A.; Bhowmick, D. *J. Colloid Interf. Sci.* **1997**, *196*, 53.
24. Graff, J.; Sanner, R. D.; Wrighton, M. S. *Organometallics* **1982**, *1*, 837.
25. (a) Buriak, J. M.; Klein, J. C.; Herrington, D. G.; Osborn, J. A. *Chem. Eur. J.* **2000**, *6*, 139. (b) Budzelaar, P. H. M.; Moonen, N. N. P.; de Gelder, R.; Smits, J. M. M.; Gal, A. W. *Eur. J. Inorg. Chem.* **2000**, 753.
26. Schrock, R. R.; Osborn, J. A. *J. Am. Chem. Soc.* **1976**, *98*, 2143.
27. Richter, B.; Spek, A. L.; van Koten, G.; Deelman, B.-J. *J. Am. Chem. Soc.* **2000**, *122*, 3945.
28. Zhang, Q.; Luo, Z.; Curran, D. P. *J. Org. Chem.* **2000**, *65*, 8866.
29. Cramer, R. *J. Am. Chem. Soc.* **1964**, *86*, 217.
30. Schenck, T. G.; Downes, J. M.; Milne, C. R. C.; Mackenzie, P. B.; Boucher, H.; Whelan, J.; Bosnich, B. *Inorg. Chem.* **1985**, *24*, 2334.
31. Sheldrick, G. M. *SHELXL: Program for Crystal Structure Refinement*; University of Göttingen: Göttingen, Germany, 1979.
32. Spek, A. L. *PLATON: A Multipurpose Crystallographic Tool*; Utrecht University, Utrecht, The Netherlands, 2001.
33. Shorter pre-hydrogenation times resulted in induction times for hydrogenation of 1-octene. Pre-hydrogenation for longer than 1 h did not change the activity of the catalyst any further.
34. (a) Landis, C. R.; Halpern, J. *J. Organomet. Chem.* **1983**, *250*, 485–490. (b) Reiss, J.; Hetflejs, J. *React. Kinet. Catal. Lett.* **1986**, *31*, 309–313.
35. Winstein, S.; Holness, N. J. *J. Am. Chem. Soc.* **1955**, *77*, 5562.